Tree-Ring Reconstruction of Streamflow by Scatterplot Smoothing

David M. Meko[1] and Katherine K. Hirschboeck[1]
[1]Laboratory of Tree-Ring Research, University of Arizona

A new modeling approach for reconstruction of streamflow from tree-ring widths is described and illustrated for the Salt-Verde River basin, Arizona. The approach, proposed to deal with relationships that are nonlinear and possibly weaker at higher flows than at low flows, includes a combination of parametric and nonparametric statistical techniques. Main steps are 1) filtering and scaling of tree-ring chronologies to adjust for lags and signal-strength differences in climate response, 2) weighting over sites to emphasize common signal for flow, and 3) interpolation of reconstructed flows from a locally weighted polynomial (loess curve) fit to the scatterplot of observed flows on the weighted tree-ring variable. Error bars for the reconstruction are derived by weighted bootstrapping of cross-validation residuals of loess-estimated flows. A comparison of reconstructions by the new method and by a more traditional approach shows important differences, especially in the inferred severity of low flows and high flows.

1. Introduction

Reconstruction of streamflow from tree rings is based on a statistically calibrated model relating a time series of observed flows to indices of tree-ring width at one or more sites. The tree-ring indices, or site chronologies (Cook et al. 1990) are viewed as proxies for moisture variations in runoff-producing parts of the watershed, and in this sense are surrogate precipitation series. The statistical model is usually multiple linear regression (MLR) and the predictors, or the chronologies, are sometimes reduced by averaging or principal components analysis, and sometimes lagged to adjust for non-climatic persistence in the tree ring series and to allow for the possibility imperfectly synchronized relationships of chronologies and flow (e.g., Stockton and Jacoby 1976; Smith and Stockton 1981; Meko and Graybill 1995; Cleaveland 2000; Meko et al. 2001; Woodhouse et al. 2006). Depending on the basin, flow transformation has been applied in such studies to mitigate problems with violations of assumptions on regression residuals. For example, log-transformation was used in reconstructions of annual flow for the Salt River (Smith and Stockton 1981), and Sacramento River (Meko et al. 2001) to deal with non-normality of residuals and non-constancy of regression error-variance, also called heteroskedasticity. As the tree-ring index, defined as the ratio of measured ring width to a fitted "age-trend", is itself an arbitrary transformation of ring width, there is no reason to expect the index to be ideally suited as a flow predictor. Flow reconstruction has indeed been reported to benefit from quadratic transformation of the tree-ring chronologies used as predictors (Cleaveland 2001). If a tree-ring index is viewed as a precipitation proxy it is reasonable to expect some sort of nonlinear relationship of the index with streamflow, as the runoff/rainfall ratio for semi-arid basins generally is not linear (e.g., Sellers 1960). Moreover, under very wet conditions the incremental increase in tree growth with increasing moisture would logically decrease, as soil moisture would no longer be the main limiting factor to growth.

Although some combination of data transformation of predictand and predictors might effectively deal with the problems mentioned above, it is important to note that transformation of the predictand is not without its own drawbacks. One is that the regression is optimized on transformed units (e.g., minimizing the sum of squares of log-transformed flow). Another is that the reconstruction must generally be back-transformed to original units if it is to be practically useful to most users (e.g., water managers), and in doing so some convenient properties of the regression estimates are lost. For example, while regression guarantees that the calibration-period means of observed and reconstructed predictand are equal, the equality no longer holds for the predictand back-transformed to original units. A third is that the error bars for reconstructed flow, while constant for the transformed flow, vary from year-to-year for back-transformed flow. A fourth drawback is that the ideal form of transform may not be obvious -- whether for straightening the flow-tree ring relationship or for reducing heteroskedasticity. Log-transformation, for example, is just one of a family of power transformations (Hoaglin et al. 1983), and its predominent use in dendrohydrology is largely due to convenience and familiarity.

The purpose of this paper is to describe and illustrate a new approach to streamflow reconstruction that circumvents flow transformation but still addresses the issues of nonlinearity and nonconstant error variance that plague reconstruction efforts, especially in smaller semi-arid basins. The approach adapts both nonparametric and robust parametric modeling to deal with some of the challenges posed by tree-ring and flow data in such basins. Tree-ring chronologies are first individually filtered and scaled to emphasize the flow signal. The resulting series are then weighted to reduce site-specific noise. Finally, reconstructed flow is interpolated from a smoothed scatterplot of observed flow on the weighted derived tree-ring variable. A confidence interval for reconstructed flows is estimated by weighted bootstrapping that reflects any increased scatter in the relationship of tree-ring index to flow as conditions become wetter.

The trial basin selected to illustrate the method is the combined Salt-Tonto-Verde basin, in south-central Arizona. We generate a reconstruction of water-year flow, 1451-1982, by the new method. That reconstruction is compared with a reconstruction by linear regression with log-transformed flow to assess the assess sensitivity of inferred hydrologic drought history to reconstruction methodology.

2. Methods

The method described here is based on an idealized relationship between flow and tree-ring index (Figure 1). The sketch might apply to a gaged or natural-flow series of annual flows, and a moisture-limited tree-ring index at a site in or near the watershed. The first relevant aspect of this idealized relationship is curvature. It is reasonable to expect that the incremental change in tree-ring index with increasing flow might decrease as conditions become so moist that soil moisture is no longer limiting to growth. The second aspect is smoothness, reflecting the likely limitation of sampled data to capture only the gross features of any relationship of tree-growth to moisture variation. The third aspect is the amplified scatter of the relationship during wet years. Amplified scatter could arise from several sources. Gaged streamflow, as derived from stage-discharge relationships, is less accurate for high flows than for low flows; this characteristic is reflected in the convention for rating stream-gage accuracy as a percentage of measured flow (e.g., Mosely and McKerchar 1993). Moreover, highs flow might also result from localized heavy rains that might or might not be commensurate with precipitation received at any particular tree-ring site. Finally, high flows may leave dramatically different imprints in the soil moisture zone of the trees depending on the intensity and duration of the contributing storms.

The conceptual idea behind the method proposed here is that a suitably smoothed scatterplot such as that in Figure 1 can be directly applied as a reconstruction model. Inference from the smoothed line can yield flow estimates in original flow units, without the need for data transformation. The procedure must of course be objective, such that the smooth curve can be regenerated by different researchers from the same basic data. The procedure must also allow for the incorporation of flow signals from multiple tree-ring sites, when the signal may differ in strength, linearity, and lag properties across sites. Finally, estimates of uncertainty of reconstructed flows must reflect the increasing scatter of the relationship at high flows.

This paper a multi-stage reconstruction modeling approach proposed for precipitation reconstruction (Meko 1997) and later adapted to flow reconstruction (Meko et al. 2001). The main extensions are incorporation of 1) quadratic regression and nonparametric smoothing to allow flexibility to handle curvilinear relationships, and 2) weighted bootstrapping to generate confidence intervals consistent with an observed amplification of reconstruction error in wetter years. The main steps are summarized in Figure 2 and are described in more detail below.

2.1 Filtering and scaling. The analysis begins with a time series of flow and a set of residual tree-ring chronologies (Cook et al. 1990). Each tree-ring chronology is first individually filtered and scaled to emphasize its signal for flow. Essentially, this step consists of multiple separate single-site reconstructions of flow, as each chronology is converted into an estimated flow time series. The statistical model for filtering and scaling is quadratic regression of flow on current and lagged tree-ring index. A contemporaneous (no lags) model is specified, followed by the possible addition of laggd terms. The contemporaneous model takes one of three possible alternative forms:

$$\begin{aligned} &1)\ y_t = b_o + b_1 w_t + b_2 w_t^2 + e_t \\ &2)\ y_t = b_o + b_1 w_t^2 + e_t \\ &3)\ y_t = b_o + b_1 w_t + e_t \end{aligned} \tag{0.1}$$

where y_t is flow in year t, w_t is the tree-ring index in year t, e_t is a noise term, and $\{b_0, b_1, b_2\}$ are parameters estimated by robust regression using the Huber weighting function. Robust regression is preferred here because of the likelihood of outliers in relating tree-growth at a particular point (single chronology) to a flow series that responds to spatially distributed runoff. While ordinary least squares minimizes the sum of squares of residuals, robust regression minimizes a weighted sum of squares of residuals, such that outliers have diminished influence on the fit (Myers 1990). Huber's weighting function assigns equal and maximum weight to observations whose residuals are within some specified threshold distance from zero, and truncates the weights for other residuals according to an influence function (Huber 1973). More details on the particular implementation of robust regression used are included in Appendix B.

The selection of model-form from the candidates in (0.1) is guided by the signs of parameter estimates from trial-and-error fitting of all three forms. Priority is given to model (1) if its parameter estimates $\hat{b}_1$ and $\hat{b}_2$ are both positive. If either estimated parameter is negative, model (1) is rejected, and whichever of (2) or (3) has the higher regression R^2 is accepted. These rules ensure that the curve is monotonically increasing and concave upward.

The filtering-and-scaling model is then expanded by adding lagged terms that may contribute significantly to the prediction accuracy. A stepwise procedure, again using robust regression with the Huber weighting function, is used to incorporate the lagged terms. If y_t is more highly correlated with the tree-ring index w_t than with the squared index w_t^2, the pool of potential lagged predictors for stepwise is $\{w_{t-2}, w_{t-1}, w_{t+1}, w_{t+2}\}$; otherwise the pool is $\{w^2{}_{t-2}, w^2{}_{t-1}, w^2{}_{t+1}, w^2{}_{t+2}\}$. Stepwise entry of lagged terms is governed by the size of the partial correlation (Mardia et al. 1979) between residuals of the model at the current step and potential predictors not yet in the model. After a lagged predictor is selected, the model is re-fit and the process is continued until all lags are entered. To avoid over-fitting, the final model selection is guided by cross-validation (leave-9-out), such that entry is truncated with the step immediately preceding the first rise in median cross-validation error. The particular choice of 9 observations for deletion in cross-validation is arbitrary, but is sufficiently large so that no cross-validation prediction relies on a tree-ring value also used to calibrate the model when the regression includes predictors lagged up to ±4 years from the year of flow.

The final filtering-and-scaling model arrived at by the procedure described above can hypothetically range in complexity from a simple linear regression of flow on the tree-ring chronology

$$y_t = b_0 + b_1 w_t + e_t \qquad (0.2)$$

to a quadratic model with four lagged terms

$$y_t = b_0 + b_1 w_t + b_2 w_t^2 + b_3 w_{t-1}^2 + b_4 w_{t-2}^2 + b_5 w_{t+1}^2 + b_6 w_{t+2}^2 + e_t\,. \qquad (0.3)$$

As each chronology is modeled separately, a different form of model may be arrived at for each tree-ring chronology in the predictor network.

The filtering-and-scaling model for a given chronology is calibrated on the full available overlap of tree-ring index and flow data, and is then applied to the longer tree-ring record to generate the long-term filtered-and-scaled tree-ring index, which extends to the start of that particular chronology. This long series can alternatively be considered a single-site reconstruction of flow, as models like (0.2) and(0.3) are reconstruction models. For brevity, the individual predicted time series $\hat{y}_t$ generated by substitution of tree-ring indices into a filtering-and-scaling regression model is referred to from here on as a SSR (single site reconstruction).

2.2 Weighting. The SSRs for the various tree-ring sites are next weighted into a single time series through principal components analysis (PCA). The PCA is run on the covariance matrix instead of the correlation matrix of the SSRs because the differing variances of the SSRs contain useful information: the variances are proportional to the percent variance of flow that could be explained by the single-site regression models. The weighted tree-ring variable can be expressed as

$$x_t = \sum_{i=1}^{i=n_c} a_i \left(\hat{y}_{t,i} - \bar{\hat{y}}_i \right) \qquad (0.4)$$

where $\hat{y}_{t,i}$ is the i^{th} SSR in year t, $\bar{\hat{y}}_i$ is the sample mean of the i^{th} SSR, a_i is the loading of principal component #1 (PC1) on the i^{th} SSR, and n_c is the number of chronologies in the network. The sample means in (0.4) are computed on the period in common period to the various SSRs. Because the PCA is run on this common period, the weighted series x_t can extend only over this period. Note that x_t is also the time series of scores of PC1 (Mardia et al. 1979), the single linear combination explaining the greatest percentage of variance of the SSRs. This time series, relying on tree-growth variations at multiple sites, is likely a more robust indicator of flow than any of the individual SSRs.

2.3 Loess-curve estimation. A scatter plot of observed flows y_t on site-weighted SSRs x_t is smoothed with locally weighted polynomial regression, or "loess" (Cleveland and Devlin 1988) such that the smoothed line is a nonparametric description of the relationship between y_t and x_t The loess model assumes generation of y by

$$y_i = g\left(x_i\right) + \varepsilon_i \tag{0.5}$$

Where ε_i are independent, normal variables with mean zero and variance σ^2, and $g\left(x_i\right)$ is some smooth function locally fit to restricted ranges of *x*. Loess begins with specification of some subset of points along the x-axis at which separate polynomial regressions of y_t on x_t are to be run. Let any one of these points be designated x_0. A regression is run on the set of observations $\{x, y\}$ with x_t nearest x_0, and in this sense the regression is "local". The user specifies the size of the desired neighborhood around x_0 as a decimal fraction of the total number of observations in the scatterplot through a smoothing parameter α. For example, $\alpha = 0.5$ specifies that the neighborhood of points for the local regression will be comprised of the 50 percent of observations with x_t nearest x_0. The larger the smoothing parameter α, the less localized the fit, and the smoother the curve. The fit is "weighted" in the sense that within the neighborhood more importance is given to observations nearer x_0 in estimating the regression parameters. We use a locally linear (polynomial degree 1) model for the loess estimation. The estimation procedure minimizes a weighted sum-of-squares of errors

$$S = \sum_{i=1}^{k} g_i\left(x_0\right)\left(y_i - \beta_0 - \beta_1 x_i\right)^2 \tag{0.6}$$

where β_0 and β_1 are regression parameters, $g_i\left(x_0\right)$ is a weighting function, and the summation is over the *k* observations in the neighborhood of x_0. The local regression procedure is repeated for a set of points x_0 distributed along the x-axis, and a predicted flow $\hat{y}_0$ is generated at each x_0. Straight-line segments joining the estimates $\hat{y}_0$ at each x_0 constitute the loess curve.

In our implementation of the loess, the target points x_0 are specified as the minimum x_t, maximum x_t and $0.05j$ quantiles of x_t, where $j = 1, \ldots, 19$. The smoothing parameter, α, is arrived at by a trial-and-error process starting with trial values {α=0.3, 0.4, 0.5, 0.6, 0.7, 0.8}. The lowest trial α giving a monotonically increasing curve is selected as the final α. This constraint, consistent with our conceptual model, requires that increasing tree-growth to be associated with increasing flow. Following Martinez and Martinez (2005), the weights g in (0.6) were computed with the tri-cube weight function (Appendix C).

2.4 Interpolation of reconstructed flows. Reconstructed flow for any given year is interpolated from the loess curve using by linear interpolation. Interpolation is necessary because the historical values of x_t will not in general coincide with an x_0 at which loess-curve estimates were made. Furthermore, extension of the loess curve beyond the extremes of x_t in the calibration period may be necessary if flow is to be inferred for years outside the calibration period. For such years, we extrapolate the loess curve linearly: a straight line between the loess curve estimates at the 0.05 quantile and minimum calibration x_t is extended to lower x_t, and a straight line between the loess curve estimates at the 0.95 quantile and maximum calibration x_t is extended to higher x_t.

2.5 Error bars for reconstructed flows. Reconstructed flows must be accompanied by some estimate of uncertainty. The conceptual model represented by the smoothed scatterplot in Figure 1 implies increased uncertainty of reconstruction with increased wetness. If the loess residuals $\hat{e}_t = y_t - \hat{y}_t$, where y_t is observed flow and $\hat{y}_t$ is flow estimated from the smoothed scatterplot, happen to be approximately normally distributed with constant variance, error bars could be estimated directly from the normal distribution. With nonconstant error variance, as in Figure 1, a theoretical approach to error bars is less tenable. We propose a heuristic approach that also does not rely on any distributional assumption on the residuals and is consistent with the observed pattern of scatter: a confidence interval for any given reconstructed flow is estimated from the cumulative distribution function of weighted-bootstrap cross-validation residuals of reconstructed flows. A time series of cross-validation residuals is first generated by the following steps: 1) the loess curve for the selected value of smoothing parameter α is repeatedly re-fit, each time leaving out a different sequence of 9 consecutive observations, 2) at each re-fitting, the loess curve is applied to predict the flow for the central of the 9 omitted observations, and 3) the residuals (observed minus predicted) from each step are assembled into a single series of residuals[1].

For any reconstructed flow, the cross-validation residuals are resampled with replacement (bootstrap) 1000 times to generate a distribution of errors tailored to that particular level of reconstructed flow. A "neighborhood" of reconstructed flows is defined based on the k reconstructed flows in the calibration period nearest the target reconstructed flow. The number k is specified as decimal fraction (e.g., 0.6) of the total number of calibration-period observations. A weighted bootstrap is used so that residuals for predicted flows closer to the target reconstructed flow are more highly represented than residuals for predicted flows further from the target. The bi-square function is used to generate the weights. The bi-square function is computed (Appendix C) and any weights less than 1/100 the maximum weight are dropped.

The 1000 noise values are then added to the reconstructed flow to generate 1000 noise-added reconstructed flow values for the target year. The $\alpha / 2$ and $1-\alpha / 2$ probability points of the empirical cumulative distribution function of the 1000 values is the $100(1-\alpha)$ percent confidence interval for the reconstructed flows. For example, the 0.10 and 0.90 probability points give the 80 percent confidence interval.

The 1000 noise-added reconstructions are also the basic data for estimating uncertainty of statistics derived from the annual reconstructions. For example, a confidence interval for 5-year running mean reconstructed flow can be directly tallied by smoothing each of the 1000 annual series with that running mean and computing the probability points of the empirical cumulative distribution function of the smoothed series in each year.

[1] Note that (2) cannot be applied to the first 4 and last 4 observations, because 9 observations are not available there for extracting central values. For those starting and ending observations, fewer than 9 observations are omitted, but a buffer of 4 observations is retained between the cross-validated observation and the nearest observation of the estimation set. For example, at the front end, observations 1-5 are omitted to get the cross-validation residual for observation 1, observations 1-6 are omitted to get the cross-validation residual for observation 2, etc.

3. Sample Application

The sample basin is the combined watersheds of the Salt, Verde and Tonto Rivers, Arizona (Figure 3). This semi-arid basin, a major source of water supply for south-central Arizona, has been the subject of previous dendrohydrologic studies (Smith and Stockton 1981; Graybill et al. 2006). Elevation in the 11,142 mi^2 (28,858 km^2) basin ranges from 637 m to 3,846 m (Hawkins 2006). The distribution of annual precipitation is bimodal, with a winter peak associated with disturbances in the westerlies, and a summer peak associated with summer convective storms (Sellers and Hill 1974). Snowmelt accounts for about 39 percent of the annual precipitation (Serreze et al. 1999). Runoff depends strongly on snowmelt (Molotch et al. 2002), and usually peaks in spring (Anderson and White 1986). Total annual precipitation is quite variable over the basin, and ranges from less than 15 inches (380 mm) in the lower elevations to more than 25 inches (635 mm) in the high mountains (Anderson and White 1986).

<u>3.2 Tree-ring data</u>. Tree-ring data for the example consists of autoregressive-residual chronologies of total ring-width for 10 sites in Arizona, western New Mexico, and southeastern Utah (Figure 3, Table 1). Field collections were made in fall of 2005 to update sites sites 1 and 2. The rest of the sites were previously collected by other researchers, and their data were obtained either from the International Tree-Ring Data Bank (ITRDB) or the Laboratory of Tree-Ring Research at the University of Arizona. The starting point for processing was measured ring widths of individual cores or cross-sections. Correlation analysis was used to identify any ring-width series with obvious dating or measuring errors, and these were eliminated from the data set. Each ring-width series was detrended with a cubic smoothing spline with amplitude of frequency response equal to 0.95 at a wavelength twice the series length (Cook and Peters 1981). Core indices were computed by the ratio method, converted to residual indices by autoregressive modeling, and then averaged over cores at the site to produce site chronologies (e.g., see Cook et al. 1990). The common period of coverage by all 10 chronologies was 1451-1983. By suggested guidelines (Wigley et al. 1984), all

chronologies were sufficiently well-replicated, with subsample signal strength exceeding 0.85 for this interval. Variance-stabilization was applied in computing each site chronology to adjust for the expected statistical dependence of the chronology variance on time-varying sample size, or number of cores (Osborn et al. 1997). Step-by-step details of the tree-ring chronology development can be found elsewhere (Appendix 3, SRP Final Report).

3.1 Flow data. The observed streamflow series, referred to as "flow" in the remainder of this paper, is the total volume of flow for the water year (October-September) summed over three gages: the Salt River near Roosevelt, the Verde River below Bartlett Dam, and the Tonto River near Roosevelt[2] (Figure 3). The flow series over 1914-2007 is highly positively skewed and has negligible autocorrelation (Table 2, Figure 4) . A characteristic of the annual flows is the occasional very high flow: flow exceeds 300 percent of the median in six years. Some periods (e.g., 1950s) are notable for a long gap between wet years.

3.3 Filtering and scaling. A comparison of basic descriptive statistics of flow and tree-ring chronologies suggests some obstacles to inferring flows from the tree-ring data (Table 2). Differences in mean or variance between flow and chronologies are unimportant to reconstruction quality, as regression methods are indifferent to linear rescaling of the variables. Skew and autocorrelation, however, deserve further attention. First-order autocorrelation is small for all series – slightly negative for the chronologies and slightly positive for the flow. Autocorrelation reaches weak significance for only one site. The negative autocorrelation for chronologies might seem surprising as these are autoregressive-residual chronologies. However it should be noted that the autoregressive (AR) models for whitening chronologies are based on the full lengths of tree-ring series, while the statistics in Table 2 are for 1914-1982, a common period later used as the reconstruction calibration period. The differing signs of autocorrelation in flow and chronologies might indicate the tree-ring data has been slightly "over-whitened" for the

[2] Some splicing of records from different gages was necessary for the Verde and Tonto series. The specific gages used are identified in Appendix 1, SRP Final Report

objective of flow reconstruction, but the small size of autocorrelations makes this a minor inconsistency.

Flow is significantly positively skewed, while eight of the ten chronologies are negatively skewed. This negative skew of chronologies is slight, and reaches significance (0.05 α-level) for only one chronology. In contrast, flow is highly positively skewed. The contrast is readily apparent in quantile-quantile plots, as illustrated for four chronologies in Figure 5. As a linear model would essentially transfer the tree-ring distribution shape onto that of the reconstructed flows, likely problems with the linear model become apparent. First is underestimation of both high and low flows. In other words, the severity of high flows would be understated, and the severity of low flows overstated. A scatter plot of flow on tree-ring index for one of the chronologies illustrates the problem: the least-squares straight line is too low at both the high-flow and low-flow ends (Figure 6A). These characteristics reflect the inability of a straight line to follow the concave curvature in the scatterplot. Another regression complication, heteroskedasticity, is indicated when the residuals from the straight-line fit are plotted against predicted flows: the classic fan-shaped pattern indicates greater variance of errors when predicted flow is high (Figure 6B).

Scatter plots of flow on other chronologies (not shown) were also more-or-less curvilinear. The robust regression modeling of flow on lagged chronologies accordingly identified quadratic models as appropriate for the scaling and filtering for each of the 10 sites (Table 3). Plots of predicted flow on tree-ring index for four of the sites for which non-lagged models were selected are shown in Figure 7. The quadratic fits are superior to straight lines in capturing the curvature of the relationships, but are notably deficient in parts of the plots, especially toward the high-flow side. For example, a more extreme curvature in the high-index side of the plot for site 4 appears necessary to track the point cluster. Signal strength as measured by the accuracy of the least squares quadratic fit varies greatly over sites – variance explained ranges from 17 to 62 percent (Table 3). All models have positive skill as measured by the reduction-of-error statistic applied in cross-validation and split-sample validation. For three of the sites, the selected filtering-and-scaling model included lags. Plots of estimated flow on the tree-ring index for those sites is of course not a smooth line because the flow estimate for a given year does not depend exclusively on the tree-ring index or its squared value in that year alone. While justified statistically in the stepwise procedure, the lags that entered are not particularly important in influencing the flow estimates. At site 1, for example, the jagged departures in the fitted line from what would be a smooth concave curve– departures imposed by the lagged predictor -- are relatively minor compared with the overall y-axis range of the fitted line (Figure 8).

3.4 Weighting. The PCA on the SSRs indicates that the first three components account for 79 percent of the variance of SSRs for their 1451-1982 common period (Table 4). PC1, which we adopt as a natural weighting function expressing common variance among SSRs, itself accounts for 63 percent of the variance. The loadings for PC1 reflect the differential signal strength in chronologies, as reflected in the variance-explained statistics for the filtering-and-scaling models listed in Table 3. For example, the site with the highest PC1 loading has the highest individual flow-variance explained, and the three sites with the lowest loadings explain the lowest percentages of flow variance. Use of PC1 as a weighting function to combine the information on flow from the various chronologies therefore most highly weights those chronologies with the strongest individual flow signal, and vice versa.

3.5 Loess-curve estimation and cross-validation. A scatterplot of observed flows on scores of PC1 of the SSRs is the framework for the loess plot. The scatterplot is repeated with loess curves corresponding to four different trial-and-error choices of smoothing parameter α in Figure 9. The loess curves for $\alpha = 0.3$ and $\alpha = 0.4$ were rejected because they were not monotonically increasing; those curves would imply decreasing flow with increasing tree-ring index for at least part of the range of tree ring index. Loess curves for $\alpha \geq 0.5$ increased monotonically, and would have been acceptable by that criterion. The curves for $\alpha = 0.5$ (not shown) was rejected for containing irregularities (not smooth enough), while the curve for $\alpha = 0.8$ was so smooth that tracking suffered at very high flows and very low flows.

The final selected loess fit (α=0.6) is plotted again in Figure 10, with a linear extension to accommodate tree-ring data outside its range encountered in the 1914-82 calibration period. This curve constitutes the nonparametric reconstruction model. Any PC1 score x_t from the tree-ring record is a pointer to the x-axis of the loess plot, and the corresponding flow is linearly interpolated from a lookup table corresponding to the loess plot. The dashed arrows on this figure illustrate the use of a the curve to infer a flow of 3.6 maf (4.4 bcm) from a PC1 score of 110.

3.6 Error bars. Weighted-bootstrap pseudo-populations of residuals and shapes of weighting functions for generating error bars for reconstructed flows are illustrated in Figure 11for four consecutive years in the 1500s. The plotted points for each of the four frames are identical, as these are just the residuals (observed flow minus predicted flow) 1914-82. The subset of those residuals bootstrapped for each reconstructed year varies, depending on the reconstructed flow. For the extremely dry year 1506, the pseudo-population comes from the left (dry) side of the plot, and consists of residuals tightly clustered around zero. In contrast, for the wet year 1509 the residuals have a much wider range.

The weighted-bootstrap sample for generating error bars differs for each year of the reconstructed as the reconstructed flow differs from year to year. The widths of the error bars consequently differ, as shown in Figure 12 for a snapshot of ten years near the start of the 16th century. Note that this snapshot includes the four years whose pseudo-populations of residuals were depicted in Figure 11. The confidence interval is narrow in 1506, reflecting the small residuals making up that pseudo-population. The interval is wider for 1507-1509, reflecting the larger residuals bootstrapped. Small differences in width of confidence interval for these years come from slight differences in the bootstrapped population and different weighting functions within those populations. The confidence interval on annual reconstructed flows accordingly varies from year to year over the full-length reconstruction (Figure 13A), and the variation carries over to any smoothed version of the reconstruction, such as the 5-year running-mean (Figure 13B). The 80% confidence interval is considerably tighter for wet periods than for dry periods (e.g., early 1600s vs 1660s.). For this particular example, the estimated record low is 0.57 maf (.70 bcm), for the period 1666-1670; the confidence interval indicates a 10 percent probability the 5-year mean flow then was as low as 0.42 maf (0.52 bcm).

3.6 Comparative reconstruction. The reconstruction generated by loess was compared with a reconstruction by linear regression. To simplify the comparison, both methods used the same ten tree-ring chronologies and calibration period. The comparison reconstruction was done using the log-10 transformed flows as a predictand, and the time series of scores of PC1 of the residual chronologies as the predictor. No lags were used in the comparison model, as these were shown to be of minor importance to the loess reconstruction.

The regression R^2 indicated that the comparison reconstruction accounted for 69% of the variance of flow in the 1914-82 calibration period. This accuracy is misleading, however, because it applies to log-transformed flows. After back-transformation to original flow units, the variance explained as computed by

$$V = 1 - \mathrm{SSE/SST} \qquad (0.7)$$

where SSE is the sum of squares of errors (observed minus predicted flows) and SST is the sum of squares of departures of observed flows from the 1914-82 mean, drops to $V = 0.59$. The corresponding value for the loess reconstruction is $V = 0.69$. The loess reconstruction by this measure is therefore a closer fit than the linear-regression reconstruction to the observed flows.

The mean, standard deviation, and skew and first-order autocorrelation of observed flows are closer to those of the loess reconstruction than to those of the linear-regression reconstruction (Table 5). The higher standard deviation for the loess reconstruction follows directly from its explaining more variance of the observed flows. Both reconstructions somewhat underestimate the very small positive first-order autocorrelation of the observed flows.

Perhaps the more interesting comparisons for alternative reconstruction methods are in the key features of the long-term reconstruction. Mean, standard deviation, skew and first-order autocorrelation are all higher for the 1451-1982 loess reconstruction than for the linear-regression reconstruction. A scatterplot of reconstructed flows by the two methods has a curvature, indicating primarily that the loess approach give greater extremes on the high-flow end and lesser extremes on the low-flow end (Figure 14). A time series plot for a snapshot of reconstructed flows in the 1500s shows that the differences in individual years are appreciable (Figure 15). For example, in wet years 1509 and 1549 the loess reconstruction is on the order of 0.5 maf (0.6 bcm) higher than the regression reconstruction. Differences in dry years are much smaller – on the order of 0.1 maf (0.1 bcm).

Cumulative distribution functions (cdfs) for the two reconstructions similarly point to the tendency for the loess reconstruction to have both higher highs and higher lows than the linear-regression reconstruction (Figure 16). For the long-term record and the 1914-82 calibration period, the cdf of the loess reconstruction is shifted to the right of the cdf of the linear regression reconstruction. The shift is most apparent in the tails.

Differences in individual years are expected to carry over to differences in multi-year flow anomalies. In Figure 17, the extremes in running means of length 1-20 years are compared. The highest running means (wettest periods) are plotted in Figure 17A, and the lowest running means (driest periods) in Figure 17B. Large differences in the two reconstructions are apparent even for running means longer than 10 years. For example, the wettest 20-year period is about 25 percent higher in flow for the loess reconstruction, and the driest 20-year period about 5 percent higher in flow for the loess reconstruction.

4. Discussion and Conclusions

Scatterplot smoothing is a useful and intuitively appealing approach to reconstruction of streamflow from tree rings when nonlinearity and heteroskedasticity of errors make linear regression problematic. An ideal setting for this approach would be a simple bivariate problem in which flow was to be inferred from a single tree-ring series – which might be an average over site chronologies. In practice, the problem is more complicated because individual tree-ring chronologies might have greatly varying strength of signal for flow, the relationships between chronologies and flow might include lags, and sites might be clustered spatially so that averaging over chronologies would unfairly emphasize some parts of the basin over others that may be of more importance to runoff. The approach presented here relies on a combination of parametric and non-parametric methods to address these complications.

The intermediate step of converting individual tree-ring chronologies to estimates of flow ("scaling and filtering") before weighting them into the predictor for the loess scatterplot runs the risk of overfitting. We attempted to minimize this risk by restricting the filtering-and-scaling models to have a fairly simple quadratic form and by using cross-validation to guard against unwarranted entry of lagged predictors.

Variations on the proposed approach might be preferable in some circumstances. In the absence of heterskedasticity of errors, the weighted bootstrapping could be omitted and reconstruction error bars generated from the error variance and some suitably fitted error distribution. A simpler approach to reduction of the individual tree-ring chronologies to a single predictor might also be possible if all chronologies showed a similarly strong signal for flow and if lagged response could be ignored. In the extreme, this might amount to the loess-curve “predictor” being merely the arithmetic average of a number of tree-ring chronologies in the basin. A less extreme departure would be to use some other form of regression model for the single-site reconstructions. We used robust regression partly based on exploratory analysis that showed some severe outliers in scatterplots of flow on individual tree-ring chronologies. Without this complication, ordinary regression, with quadratic or some other power-transformation of the tree-ring indices, might be preferred. Another possibility would be generate the single-site reconstructions by loess curves (scatterplot smoothing) instead of quadratic regression. We chose not to do that in the interest of automating the reconstruction process: for reconstruction problems with many tree-ring chronologies, the scatterplot smoothing was judged to be too tedious in requiring a large number of subjective decisions (e.g., on smoothing parameters for individual scatterplots).

The method described here can be readily extended to accommodate time-nested tree-ring reconstruction models (e.g., Meko et al. 2001) . For brevity, we have restricted the sample application to reconstruction for a specific time period uniformly covered by all the tree ring chronologies. In practice, some subset of chronologies will extend much further back in time, and some may come nearly up to present. For those situations, the modeling procedure would simply be repeated such that multiple reconstructions were generated. If these happened to overlap, as is usual, priority could be given in assigning the final reconstructed flow for a given year to the model deemed superior in some way (e.g., lowest validation error variance).

The proposed approach is perhaps most blatantly subjective in selection of the smoothing parameter α for the loess curve. Our conceptual model dictated constraints on this choice. The conceptual model is that trees grow faster as conditions become wetter, but may respond less to increased moisture under very wet conditions: we accordingly assume the curve fit to a scatterplot of flow on tree-ring index should increase monotonically, and perhaps increase in steepness toward high flows. These constraints would perhaps not apply in some studies. For example, situations could be envisioned in which very moist conditions become detrimental to growth. Besides the smoothing parameter, the other parameter typically varied in loess smoothing is the degree- of-polynomial, λ (Martinez and Martinez 2005). We choose a locally linear model, corresponding to $\lambda = 1$. The locally-linear model has been recommended for having well-behaved end-effects (Martinez and Martinez 2005). The loess curve by the local-linear model could also be readily extended to allow estimation of flow for those years with tree-ring data outside its calibration-period range.

The confidence intervals from weighted-boostrapping of cross-validation residuals are of course not exactly reproducible, as a bootstrap sampling will generate a different sample when repeated. The size of the bootstrap sample (e.g., 1000 vs 5000) will affect the repeatability of the confidence interval; an optimal size for particular problems could be fine-tuned with Monte Carlo sensitivity studies. Another limitation that should be mentioned is the violation of the regression assumption of constant error variance. This violation makes can affect properties (e.g., bias, variance) of estimated regression predictors coefficients, and have important implications for hypothesis testing using those coefficients (e.g., Kennedy 2003). Inferences based on significance of coefficients is not an issue in flow reconstruction. The degree to which the violation negatively impacts the predictions in a flow reconstruction model is unknown. The most important points in the reconstruction application are that 1) the smooth curve gives and acceptable and reasonably robust fit to the scatterplot, and 2) the error bars reflect any systematic dependence of reconstruction accuracy on level of predicted flow.
Application of the method presented here should include cross-validation and graphical quality control to ensure that these points are addressed. Alternatively, data transformation could be investigated in combination with the loess approach to

circumvent the problem of heteroskedasticity of errors – with the tradeoff of likely need for backtransformation to make reconstructed flows usable.

The reconstruction approach proposed here is not claimed to be superior in general to any existing statistical reconstruction method, but is proposed as a useful alternative for reconstruction scenarios plagued by nonlinearity of relationships and heteroskedasticity of errors. The scenario is most likely in small, semi-arid basins, where flashy flow regimes may produce highly-skewed flows and where high flows are unlikely to leave a footprint in tree-growth commensurate with the flow anomaly. Comparative exercises can point out sensitivity of major reconstructed time series features to choice of reconstruction method. Our limited comparison with a more convention linear-regression reconstruction model indicates the loess procedure as implemented here does give practically significant differences in reconstructed features. The more extreme highs and less extreme lows by the loess reconstruction are a direct consequence of the effort to deal with curvature in the relationship between tree-ring index and flow. Other types of statistical models, not investigated here, may be applicable to flow-reconstruction problems in which the data are not particularly well-suited for regression. Response surfaces (Graumlich 1993), neural networks (Zhang et al. 1999; Woodhouse 1999; Ni et al. 2002), and classification trees (Meko and Baisan 2001) are some of the other techniques that have been used to deal with nonlinearity in tree-ring reconstruction models.

Acknowledgements. This work was supported by the Salt River Project.

References

Anderson, T., and White, Natalie D., 1986, Arizona Surface-Water Resources, National Water Summary 1985 -- Hydrologic events and surface-water resources, United States Geological Survey Water-Supply Paper 2300, 145-150.

Box, G.E.P., and Jenkins, G.M., 1976, Time series analysis: forecasting and control: San Francisco, Holden Day, p. 575 pp.

Cleaveland, M.K., 2000, A 963-year reconstruction of summer (JJA) streamflow in the White River, Arkansas, USA, from tree rings: The Holocene, v. 10, no. 1, p. 33-41.

Cleveland, W.S., and Devlin, S.J., 1988, Locally weighted regression: An approach to regression analysis by local fitting: Journal of the American Statistical Association, v. 83, no. 403, p. 596-610.

Cook, E.R., Briffa, K., Shiyatov, S., and Mazepa, V., 1990, Tree-ring standardization and growth-trend estimation, *in* Cook, E.R., and Kairiukstis, L.A., eds., Methods of Dendrochronology, Applications in the Environmental Sciences: Kluwer Academic Publishers, p. 104-123.

-----, and Peters, K., 1981, The smoothing spline: A new approach to standardizing forest interior tree-ring width series for dendroclimatic studies, Tree-Ring Bulletin 41, 45-53.

Graumlich, L., 1993, A 1000-year record of temperature and precipitation in the Sierra Nevada, Quaternary Research 39, 249-255.

Graybill, D.A., Gregory, D.A., Funkhouser, G.S., and Nials, F.L., 2006, Long-term streamflow reconstructions, river channel morphology, and aboriginal irrigation systems along the Salt and Gila Rivers, In: Environmental Change and Human Adaptation in the Ancient Southwest, edited by Jeffrey S. Dean and David E. Doyel. University of Utah Press.

Hawkins, T.W., 2006a, Parameterization of the snowmelt runoff model for the Salt-Verde system, Arizona, during drought conditions: Journal of the Arizona-Nevada Academy of Science, v. 380, no. 2, p. 63-73.

Hoaglin, D.C., Mosteller, F., and Tukey, J.W., 1983, Understanding Robust and Exploratory Data Analysis: John Wiley & Sons, Inc., New York, p. 447.

Huber, P.J., 1973, Robust regression: Asymptotics, conjectures, and Monte Carlo: Annals of Statistics, v. 1, p. 799-821.

Kennedy, P., 2003, A guide to econometrics: Cambridge, Massachusetts, The MIT Press.

Mardia, K., Kent, J., and Bibby, J., 1979, Multivariate Analysis: Academic Press, 518.

Martinez, W.L., and Martinez, A.R., 2005, Exploratory data analysis with MATLAB: New York, Chapman & Hall/CRC.

Meko, D.M., 1997, Dendroclimatic reconstruction with time varying subsets of tree indices: Journal of Climate, v. 10, p. 687-696.

-----, and Baisan, C.H., 2001, Pilot study of latewood-width of confers as an indicator of variability of summer rainfall in the north American Monsoon region: International J. of Climatology, v. 21, p. 697-708.

-----, and Graybill, D.A., 1995, Tree-ring reconstruction of Upper Gila River discharge: Water Resources Bulletin, v. 31, no. 4, p. 605-616.

-----, Therrell, M.D., Baisan, C.H., and Hughes, M.K., 2001, Sacramento River flow reconstructed to A.D. 869 from tree rings: J. of the American Water Resources Association, v. 37, no. 4, p. 1029-1040.

Michaelsen, J., 1987, Cross-validation in statistical climate forecast models, J. of Climate and Applied Meterorology 26, 1589-1600.

Molotch, N.P., Fassnacht, S.R., Helfrich, S.R., and Bales, R., C., 2002, Estimating the distribution of snow water equivalent and snow extent beneath the cloud-cover in the Salt-Verde river basin, Arizona: 59th Eastern Snow conference, Stowe, Vermont USA.

Mosely, M.P., and McKerchar, A.I., 1993, Streamflow, *in* David R. Maidment, ed., Handbook of Hydrology: McGraw-Hill Book Company.

Myers, R.H., 1990, Classical and modern regression with applications, second edition: Pacific Grove, California, Duxbury.

Ni, F., Cavazos, T., Hughes, M.K., Comrie, A.C., and Funkhouser, G., 2002, Cool-season precipitation in the southwestern USA since A.D. 1000: Comparison of linear and nonlinear techniques for reconstruction: International Journal of Climatology, v. 22, p. 1645-1662.

Osborn, T.J., Briffa, K.R., and Jones, P.D., 1997, Adjusting variance for sample-size in tree-ring chronologies and other regional mean timeseries: Dendrochronologia, v. 15, p. 89-99.

Sellers, W.D., and Hill, R.H., 197, Arizona Climate 1931-1972, The University of Arizona Press, Tucson, Arizona, 616 pp.

Serreze, M., Clark, Armstrong, R.L., McGuiness, D.A., and Pulwarty, R.S., 1999, Characteristics of the western United States snowpack from snowpack telemetry (SNOTEL) data: Water Resources Research, v. 35, no. 7, p. 2145-2160.

Smith, L.P., and Stockton, C.W., 1981, Reconstructed streamflow for the Salt and Verde Rivers from tree-ring data: Water Resources Bulletin, v. 17, no. 6, p. 939-947.

Stockton, C.W., and Jacoby, G.C., 1976, Long-term surface-water supply and streamflow trends in the Upper Colorado River Basin, Lake Powell Research Project Bulletin No. 18: National Science Foundation, 70 pp.

Wigley, T.M.L., Briffa, K.R., and Jones, P.D., 1984, On the average value of correlated time series, with applications in dendroclimatology and hydrometeorology: Journal of Climate and Applied Meteorology, v. 23, p. 201-213.

Woodhouse, C.A., 1999, Artificial neural networks and dendroclimatic reconstructions: An example from the Front Range, Colorado, USA: The Holocene, v. 9, no. 5, p. 521-529.

Zhang, Q.-B., Hebda, R.J., Zhang, Q.-J., and Alfaro, R.I., 1999, Modeling tree-ring growth responses to climatic variables using artificial neural networks: Forest Science, v. 46, no. 2, p. 229-238.

Appendix A. Statistical software

All computations were done in MATLAB©, using a combination of functions written by us and available from MATLAB© and the Computational Statistics Toolbox (Martinez and Martinez 2002). Numerous user-written functions and scripts were also used in the analysis.

Appendix B. Robust Regression and Huber Weighting Function

In linear regression the predictand for any given observation or year i is modeled as

$$y_i = \mathbf{x}_i{}'\mathbf{b} + e_i, \qquad i = 1, 2, \ldots, n \tag{1.1}$$

where y_i is the predictand, $\mathbf{x}_i$ is a row vector of predictors, $\mathbf{b}$ is a vector of coefficients, and e_i is the noise. Predictions can be generated by $\hat{y}_i = \mathbf{x}_i{}'\hat{\mathbf{b}}$, where the "hat" denotes estimated values, such that the residuals $\hat{e}_i$ are defined as

$$\hat{e}_i = y_i - \hat{y}_i \tag{1.2}$$

While ordinary least squares regression seeks to minimize $\sum_{i=1}^{n} \hat{e}_i^2$, robust regression seeks to minimize $\sum_{i=1}^{n} w_i \hat{e}_i^2$ where w_i are weights that can be used discount the importance of outliers in the fit (Myers 1990).

Robust regression with the Huber function was implemented with MATLAB function `robustfit`. An ordinary least squares fit (non-robust) is first run, and the diagonals of the "hat" matrix, $h_{i,j}, \quad j = i$ stored. (The "hat" has been dropped from the estimated quantities in the following to avoid clutter.) Scaled residuals are then computed as

$$r_i = \frac{e_i}{a\hat{\sigma}\sqrt{1 - h_{i,i}}} \tag{1.3}$$

where $a = 1.345$ is a specified Huber "tuning factor", and

$$\hat{\sigma} = \frac{\mathrm{MED}\left(\left|e_i\right|\right)}{0.6745} \tag{1.4}$$

is a scale factor reflecting the variability of the residuals. The Huber weights are given by

$$w_i = \begin{cases} 1; & |r| \le 1 \\ 1/|r|; & |r| > 1 \end{cases} \qquad (1.5)$$

The robust estimates of regression parameters are derived iteratively:

1) Run an ordinary least squares to obtain initial, non-robust, parameter estimates $\mathbf{b}_0$, initial residuals $e_{i,0}$, and diagonal elements of the hat matrix, $h_{i,i}$
2) Using those residuals, compute the initial scaled residuals $r_{i,0}$ from (1.3) and initial weights $w_{i,0}$ from (1.4) and (1.5)
3) Use weighted least squares (e.g., Weisberg 1985)to get new robust parameter estimates $\mathbf{b}_{R0} = \left(\mathbf{X}'\mathbf{W}_0\mathbf{X}\right)^{-1}\mathbf{X}'\mathbf{W}_0\mathbf{y}$, where $\mathbf{W}_0$ is a diagonal matrix of weights with ith diagonal element $w_{i,0}$
4) Let the parameter estimates from step 3 take the role of starting parameters, and apply (1.3), (1.4), and (1.5) to get new residuals, a new value of $\hat{\sigma}$, and new weights
5) Go back to step 3
6) Repeat steps 3 and 4 until convergence is reached

In function `robustfit`, the constant 0.6745 makes the estimate unbiased for the normal distribution. If there are *p* columns in X, the smallest *p* absolute deviations are excluded when computing the median absolute residual, $\mathrm{MED}\left(|e_i|\right)$. Convergence is assumed when the maximum change in any of the parameters from the previous step is very small -- does not exceed some specified small number (tied to the machine precision). The iteratively reweighted least squares is otherwise continued to a maximum possible 50 iterations,

Appendix C. Bisquare and tri-cube weighting functions

The bisquare and tri-cube weighting functions are described in the context of robust statististics by Martinez and Martinez (2005). Given a set of observations $\{x_i, y_i\}$ and some arbitrary point x_0 on the x-axis, define the k nearest neighbors as the k points with x_i closest to x_0. Define the relative distance of any observation from x_0 as

$$u = \frac{|x_0 - x_i|}{\Delta_k(x_0)} \tag{1.1}$$

where $\Delta_k(x_0)$ is the largest $|x_0 - x_i|$ for any of the k nearest neighbors. The bisquare weights are

$$w_i(x_0) = \begin{cases} (1-u^2)^2; & 0 \le u < 1 \\ 0; & \text{otherwise} \end{cases} \tag{1.2}$$

and the tri-cube weights are

$$w_i^*(x_0) = \begin{cases} (1-u^3)^3; & 0 \le u < 1 \\ 0; & \text{otherwise} \end{cases} \tag{1.3}$$

Equations (1.2) and (1.3) along with the definition of u specify that the weight decreases from a maximum for the observation nearest x_0 to zero for the farthest observation in the neighborhood, and remains zero for any observation outside the neighborhood. Weights are cannot be less than zero or greater than 1, and a weight 1 occurs only if some observation happens to have an x-value exactly at x_0. The bisquare and tri-cube weighting functions both decline with a sigmoid shape, but steepness of decline differs such that the tri-cube weights are higher than the bisquare weights for points near x_0 and lower than the bisquare weights for points far from x_0 (Figure ??).

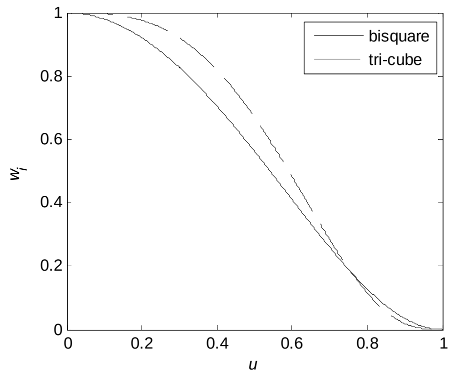

Figure 1. Bisquare and tri-cube weights as a function of relative distance (see text).

Table 1. Site information on tree-ring chronologies.

N[a]	Name[b]	Species[c]	Location[d] Lat	Lon	El(ft)	N_{tree}[e]	Period[f]		s[g]
1	Wahl Knoll	PSME	34.0	-109.4	9367	23(3)	1435	2005	a
2	Black Mtn	PSME	33.4	-108.2	8721	41(8)	1327	2005	a
3	Navajo Mtn	PIED	37.0	-110.8	7384	13(6)	1330	1989	b
4	Kane Springs	PIED	37.5	-109.9	6350	26(5)	1361	1988	b
5	Betatakin Cyn	PSME	36.7	-110.5	6599	26(9)	1306	1989	b
6	Walnut Cyn	PIPO	35.2	-111.5	6696	17(2)	1451	1987	b
7	Spider Rock	MIX	36.1	-109.3	6105	25(6)	1399	1989	b
8	Satan Pass	PSME	35.6	-108.1	7384	17(2)	1410	1990	b
9	Dinnebito	PIED	36.2	-110.5	6202	28(6)	1410	1983	b
10	El Malpais	PSME	35.0	-108.1	7826	21(16)	1100	1990	c

[a]Site as numbered on map

[b]Site name

[c]Species: PSME=Pseudotsuga menziesii; PIED= Pinus edulis
PIPO=Pinus ponderosa; Mix = mix of PSME and PIPO

[d]Location: latitude and longitude in decimal degrees, elevation
in feet above sea level

[e]Maximum number of trees in any year (number in 1541)

[f]Start and end year of site chronology

[g]Source of data: a=site updated by D. Meko in July 2005;
b=Southwest Archaeology Project (J. S. Dean);
c=Site collected by H. Grissino-Mayer (ringwidths are subset of
file nm572.rwl downloaded from Internation Tree-Ring Data Bank

Table 2. Statistics of annual flows and tree-ring chronologies.

Series[a]	Mean	Std Dev	Skew	Normal	r(1)
	Statistics[b]				
Flow	1.201	0.8521	1.50**	F**	0.12
Site 1	1.001	0.1515	-0.22	P	-0.17
Site 2	1.009	0.2372	-0.25	P	-0.15
Site 3	0.984	0.2371	-0.02	F*	-0.06
Site 4	0.984	0.1987	-0.38	P	-0.18
Site 5	1.007	0.1869	-0.36	P	-0.11
Site 6	1.027	0.2239	-0.53*	P	-0.06
Site 7	1.002	0.2057	-0.09	P	-0.18
Site 8	0.999	0.2794	0.30	P	-0.15
Site 9	1.018	0.2454	0.06	P	-0.07
Site 10	1.002	0.2951	-0.04	P	-0.19*

[a]Series: first series is annual flows, others are residual tree-ring chronologies as numbered on map in Figure 2

[b]Statistics are the mean, standard deviation, skewness, Lilliefors test for normality, and first-order autocorrelation. Significance at 0.05 and 0.01 alpha-levels are flagged by "*" and "**". Flow statistics (mean and standard deviation) are in millions of cubic feet, and index statistics are dimensionless. Analysis period is 1914-82.

Table 3. Summary statistics of filtering-and-scaling models for tree-ring chronologies.

N[a]	Model[b]	VE[c]	Cross-validation[d] RMSE (maf)	MAE (maf)	MedAE (maf)	Split-sample[e] RE	REA	REB
1	2:2000	0.26	25.2	15.6	8.4	0.17	0.23	0.23
2	2:0000	0.17	25.9	16.5	10.0	0.12	0.10	0.26
3	2:0000	0.46	20.8	13.9	9.5	0.38	0.49	0.41
4	2:0000	0.36	22.4	14.8	8.6	0.28	0.42	0.29
5	2:0000	0.34	22.3	14.9	10.1	0.29	0.43	0.22
6	2:0002	0.31	23.9	16.0	9.5	0.22	0.20	0.40
7	2:0000	0.41	21.7	13.8	8.1	0.32	0.49	0.29
8	2:0000	0.40	22.4	15.1	9.9	0.28	0.40	0.40
9	2:0020	0.62	19.0	13.7	9.8	0.50	0.57	0.65
10	12:0000	0.23	24.8	17.0	11.1	0.12	0.25	0.13

[a]N: sites number as used on map

[b]Model: code defining regression model of flow on current and lagged tree-ring index; digits before colon indicate power(s) of current-year index (e.g., 2 denotes 'squared'); columns after colon indicate powers on index at lags t-1, t-2, t+1 and t+2 years relative to the year of flow

[c]VE: variance-explained statistic computed from observed and predicted flows on the loess plot. The statistic is defined as VE= 1-SSE/SST, where SSE is the sum of squares of differences of observed flows and predicted flows and SST is the sum of squares of departures of observed flows from their mean.

[d]Cross-validation: statistics from leave-9-out cross-validation of the loess curve. RMSE=root mean square error; MAE=mean absolute error; MedAE=median absolute error; RE=reduction-of-error statistic (see text)

[e]Split-sample: Reduction-of-error statistics from split-sample calibration-validation with calibration on first half of data and validation on second half (REA) and for calibration on the second half and validation on the first half (REB)

Table 4. Summary of principal components analysis on filtered and scaled tree-ring chronologies, 1451-1982. Table truncated to include only first three components accounting for cumulative 79 percent of variance.

	Loadings		
Site[a]	PC#1	PC#2	PC#3
1	0.178	0.407	-0.416
2	0.190	0.366	-0.090
3	0.394	-0.315	0.381
4	0.358	-0.192	0.163
5	0.295	0.018	0.238
6	0.308	-0.144	-0.638
7	0.333	0.234	-0.059
8	0.289	0.414	0.357
9	0.478	-0.398	-0.201
10	0.207	0.398	0.108
Var	62.7	10.8	5.4

[a]Site: First 10 rows correspond to tree-ring sites as numbered on map in Figure 2 and listed in Table 1. Last row is percentage of variance accounted for by the PC

Table 5. Summary statistics observed flows and flows reconstructed by two alternative methods.

Period	Mean	Stdev	Skew	r(1)
	Statistics[a]			
1914-1982				
Loess	1.229	0.698	0.92	0.01
Regr	1.112	0.556	0.66	-0.06
Obs	1.201	0.852	1.50	0.12
1541-1982				
Loess	1.229	0.699	1.08	0.05
Regr	1.102	0.553	0.73	0.01

[a]Statistics: mean (maf), standard deviation and first-order autocorrelation

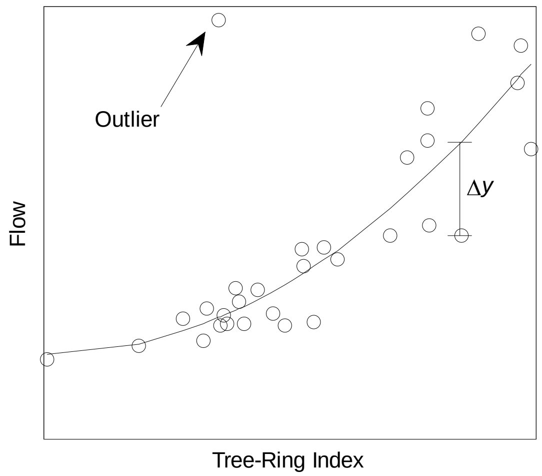

Sketch of idealized relationship between tree-ring index and annual streamflow for a tree-ring chronology in a semi-arid watershed. Growth-response to additional moisture flattens at high moisture levels, leading to concave curvilinear scatter. Relationship weakens as moisture increases, leading to larger "errors" (**Δy**), or departures from fitted smooth line, for high flows. Smoothed line is quadratic fit to data with the outlier omitted.

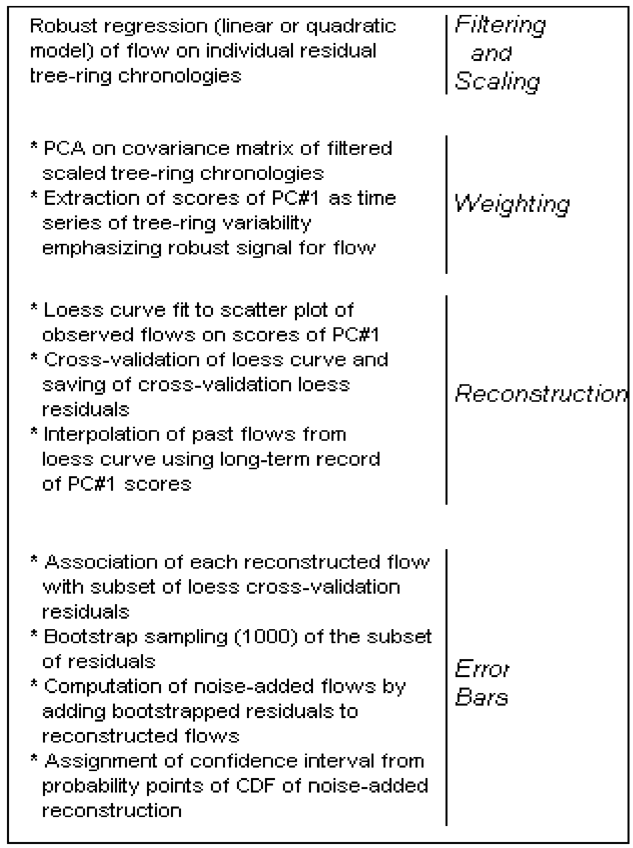

Figure 2. Flowchart summarizing main steps in reconstruction method.

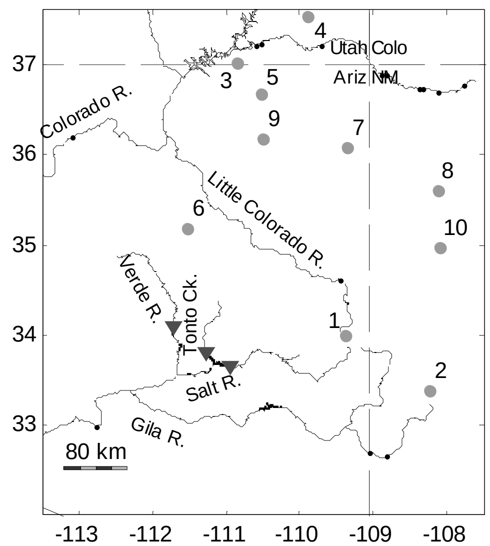

Figure 3. Map showing locations of tree-ring sites (circles) and gages (triangles) used in sample reconstruction of sum of annual flows of Salt, Verde and Tonto Rivers. Tree-ring sites numbered as in Tables 1 and 2.

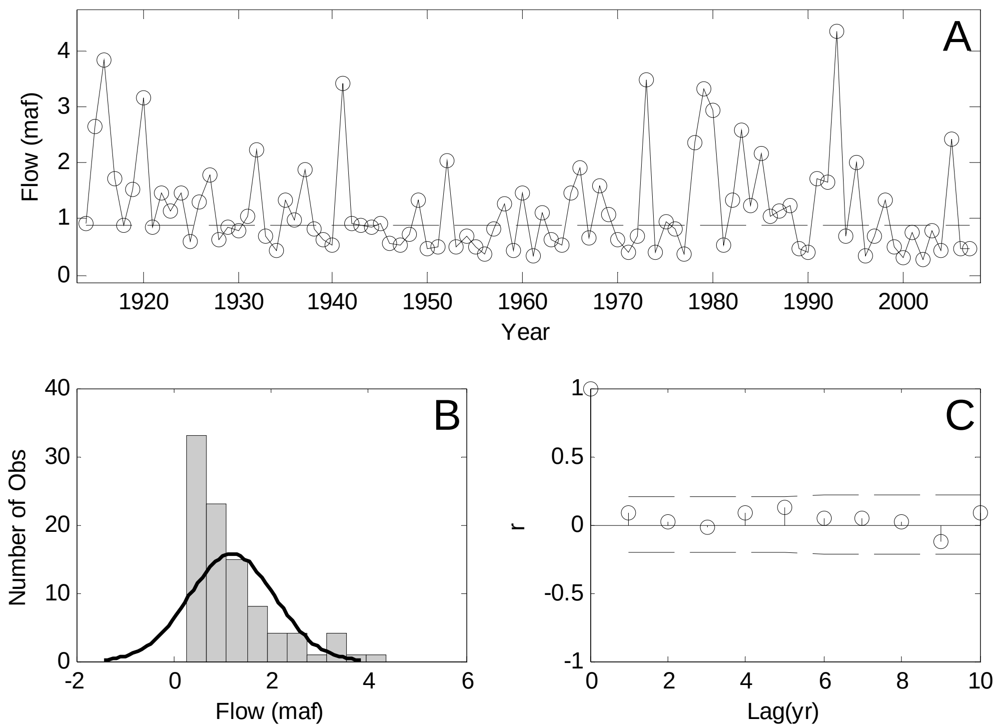

Figure 4. Statistical characteristics of observed water-year total flows, 1914-2007. (A) Time series plot, with dashed horizontal line at 1914-2006 median. (B) Histogram with superposed pdf of theoretical normal distribution. (C) Autocorrelation function with 95% confidence interval defines as two time the large-lag standard error (Box and Jenkins 1976).

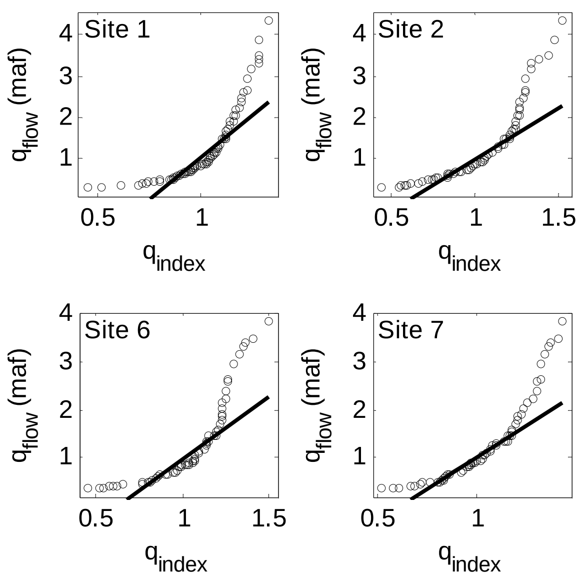

Figure 5. Quantile-quantile plots illustrating diffences in shapes of distributions of annual flows and tree-ring indices. Flow series is SVT water-year total. Tree-ring series are residual chronologies (Cook et al. 1990) for four sites in study are (numbered as in Figure 3 and Table 1).

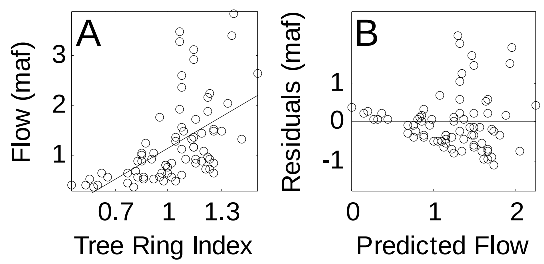

Figure 6. Scatter plots illustrating effects of nonlinearity and non-variance of errors in reconstruction by simple linear regression of flow on untransformed tree-ring index. (A) observed flows against tree-ring index. (B) regression residuals against flows generated by simple linear regression model. Data are SVT flows and chronology #6 (Table 1, Figure 3) for common period 1914-87.

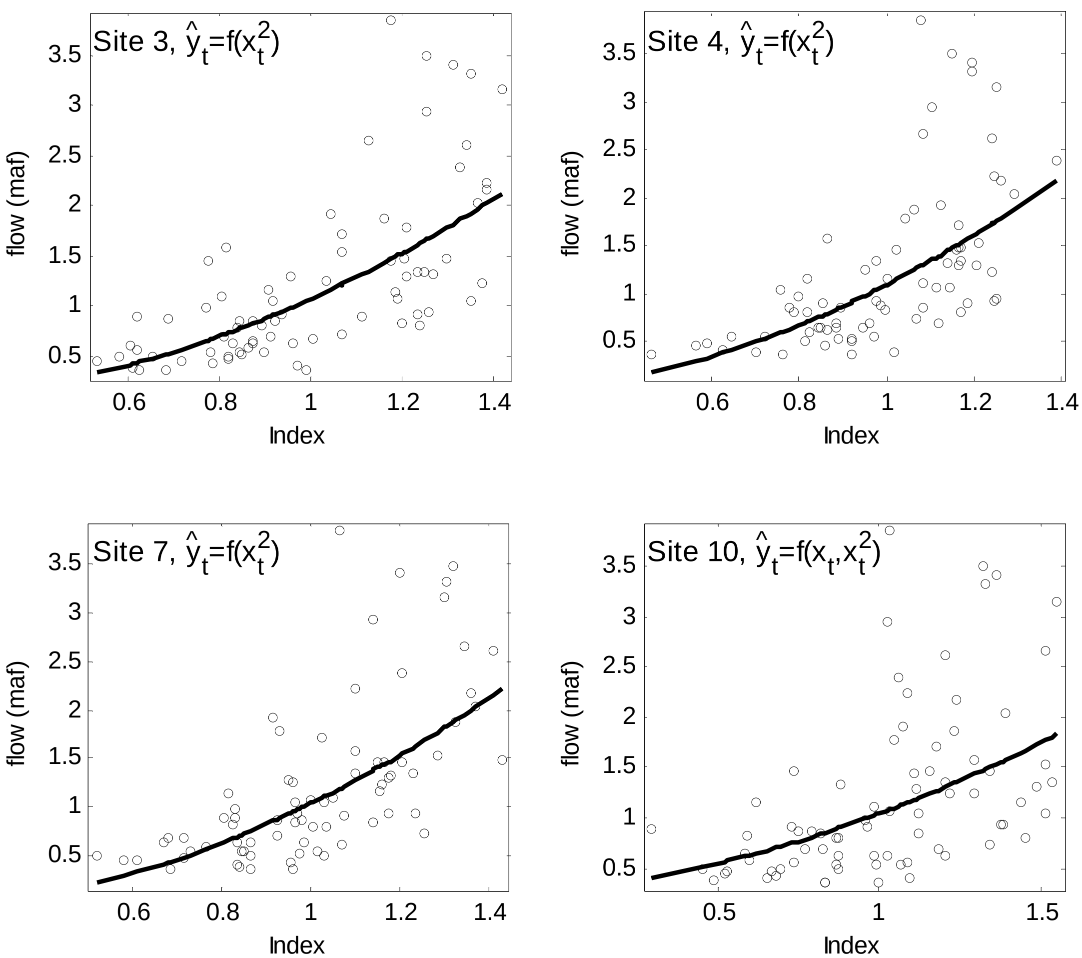

Figure 7. Sample scatterplots and predictions from quadratic robust regression models scaling and filtering tree-ring chronologies into estimates of flow. Sites numbered as in Figure 3 and Table 1. Models for all ten sites listed in Table 3.

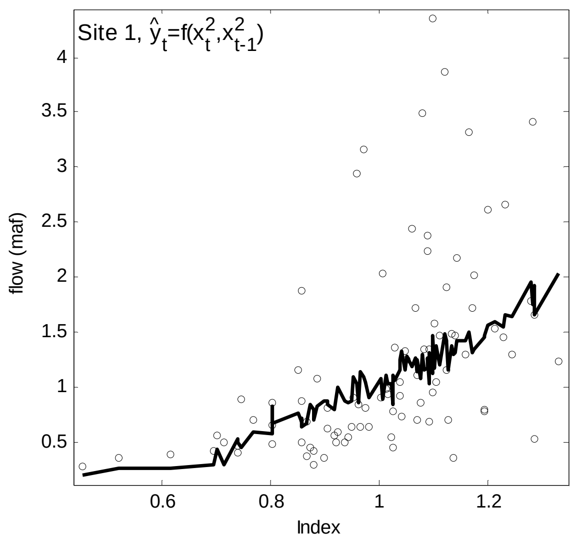

Figure 8. Scatterplot of flow on tree-ring chronology for a site with a lagged predictor in the quadratic regression model. Remainder of caption as Figure 7.

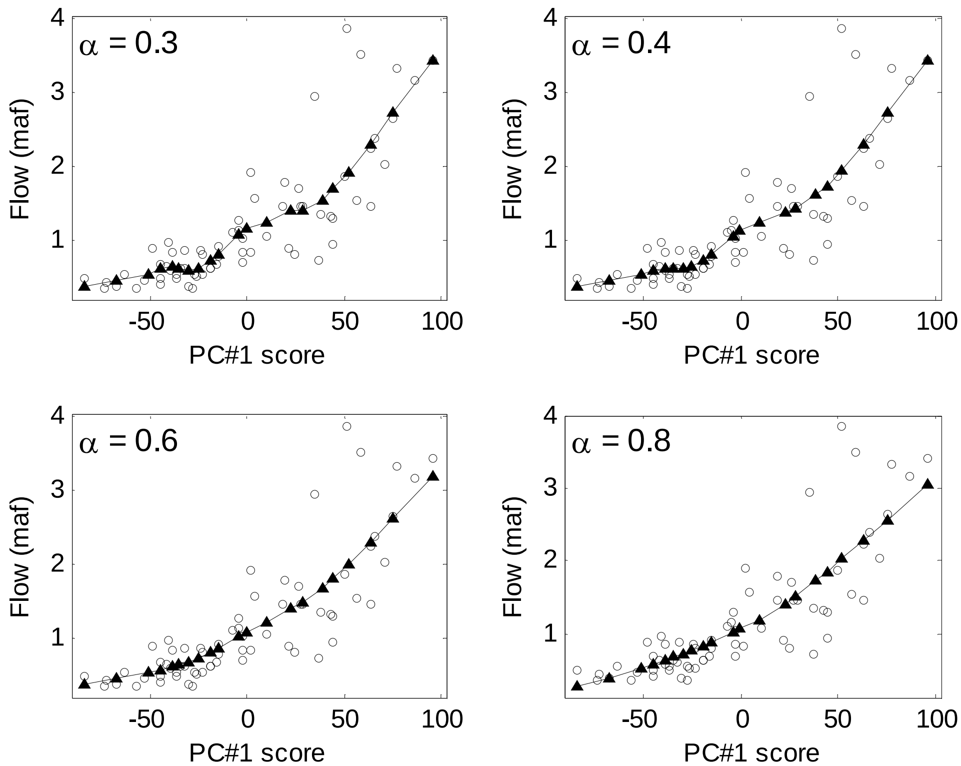

Figure 9. Plots illustrating change in smoothness of loess plot with change in smoothing parameter, α. Open circles are observed data. Loess curve is composed of straight line segments connecting triangles located at minimum, maximum, and 0.05, 0.10, …, 0.95 quantiles of PC#1 scores. Analysis period 1914-82.

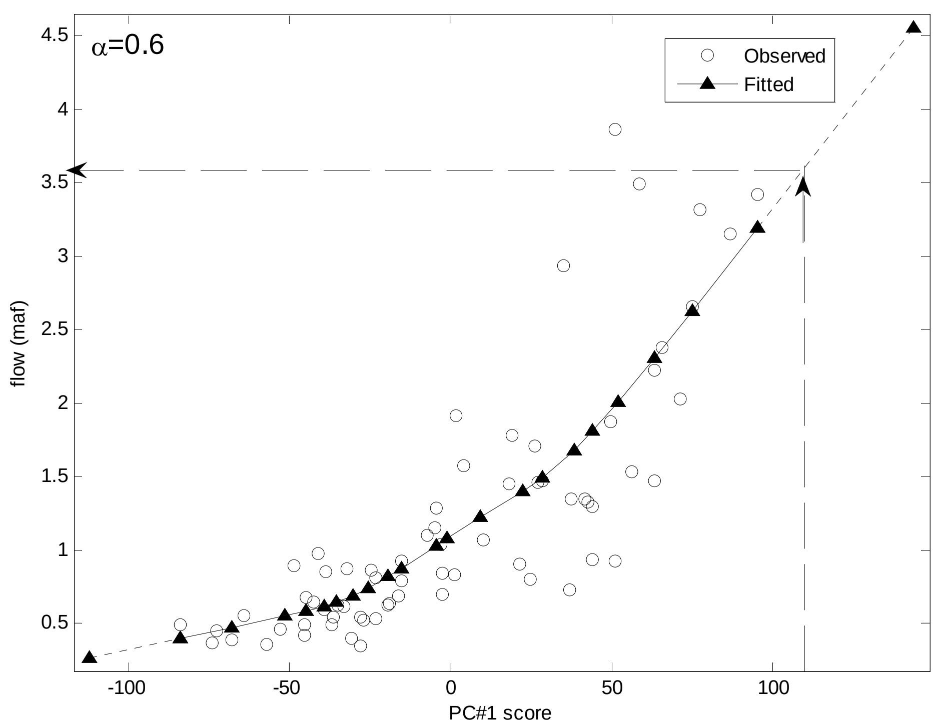

Figure 10. Loess curve used for interpolating final reconstruction. Dotted line is linear extension to allow interpolation outside the range of data in the 1914-1982 loess calibration period. Arrows illustrate using the loess curve to infer a flow of 3.6 maf from a PC#1 score of 110.

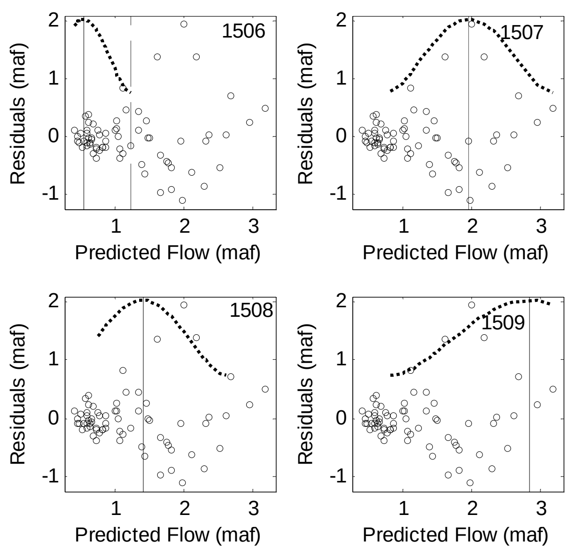

Figure 11. Weighted-bootstrap pseudo-populations of residuals for reconstructed flows in 1506-1509. Circles mark residuals for the 1914-82 model calibration period plotted against predicted flows. Solid vertical line drawn at the reconstructed flow for year annotated at upper right. Residuals used for weighted bootstrapping in annotated year are those in section of x-axis spanned by dotted curve. Height of dotted curve is proportional to weights assigned in the weighted bootstrapping (declines to weight of zero at ends of curve).

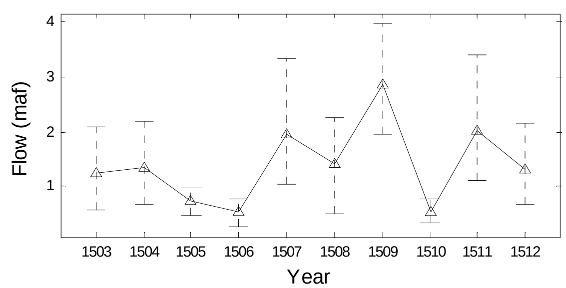

Figure 12. Ten-year segment of reconstruction with weighted-bootstrap 80% confidence intervals.

.

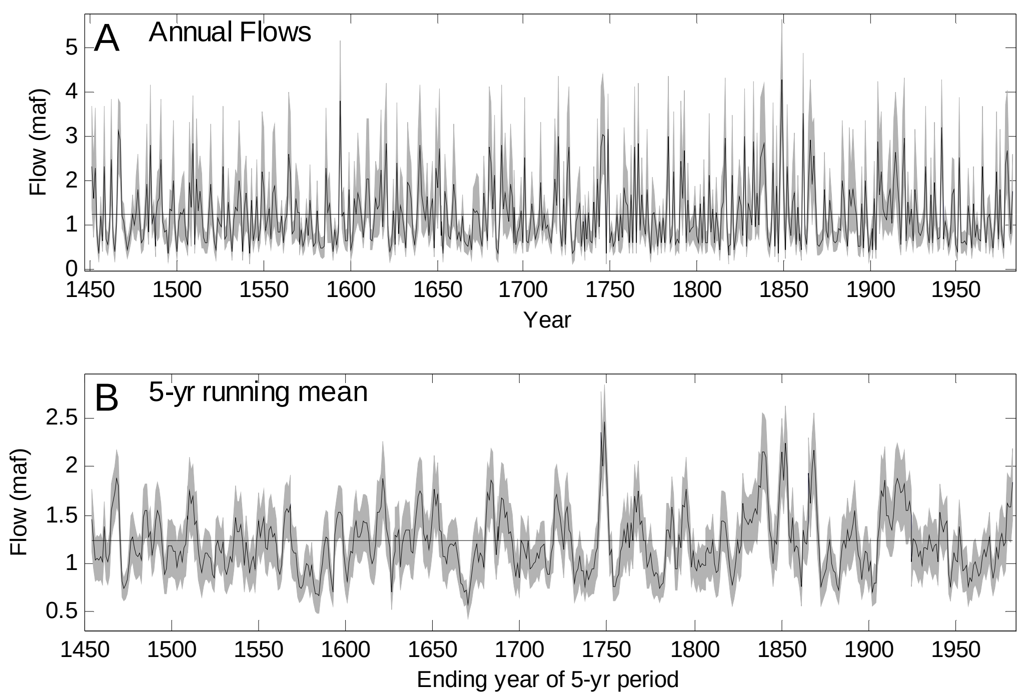

Figure 13. Time series plots of annual reconstructed flows with 80 percent confidence interval. (Top) Annual flows, 1541-1982. (Bottom) Five-year running mean of annual flows. Horizontal line in both plots is the 1541-1982 mean of annual reconstruction.

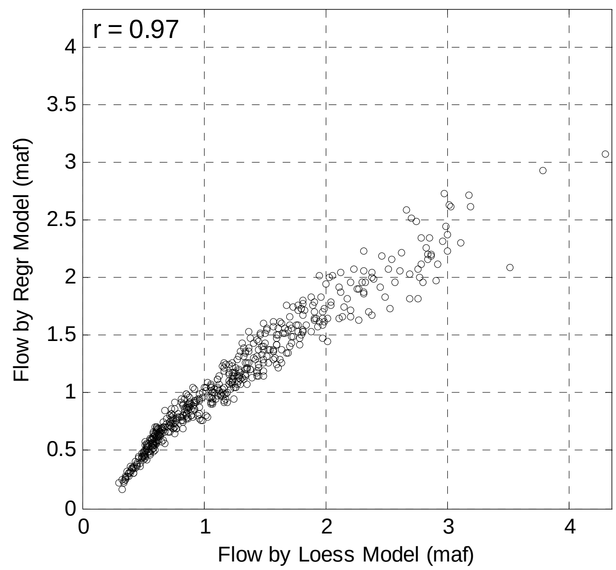

Figure 14. Scatterplot of reconstructed flows by linear regression model on reconstructed flows by loess model, 1451-1982.

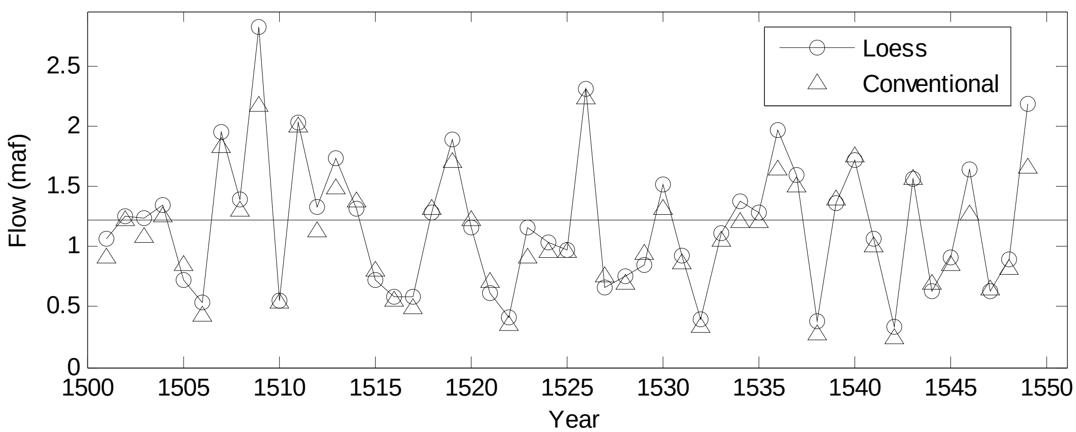

Figure 15. Fifty-year time series segment comparing annual reconstructed flows by loess model with those by conventional model. Conventional model is linear regression of flow on scores of first principal component of the 10 residual tree-ring chronologies.

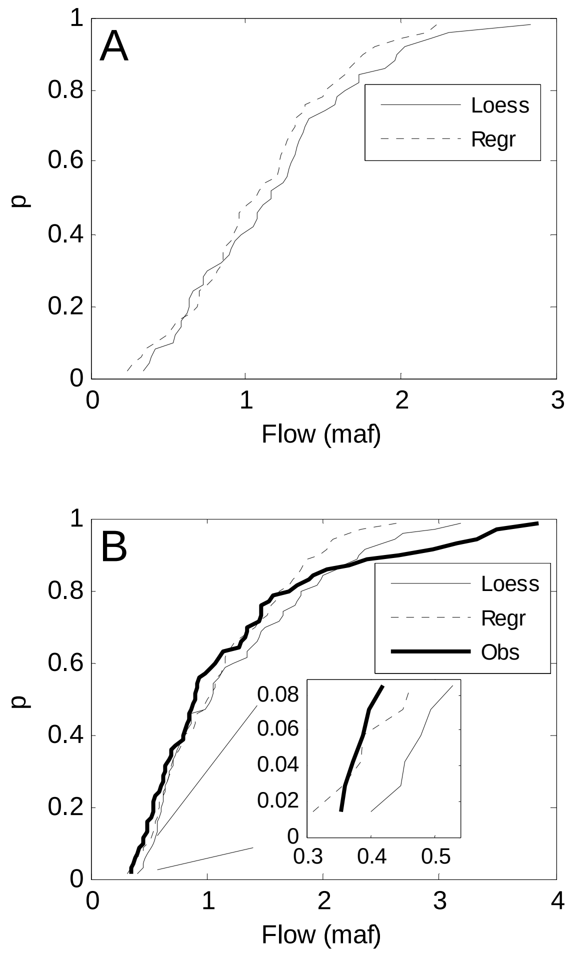

Figure 16. Empirical cumulative distribution functions (cdf's) comparing distributions of flows. (A) full reconstruction period (1451-1982). (B) model calibration period (1914-1982). Cdf for observed flows also shown in (B).

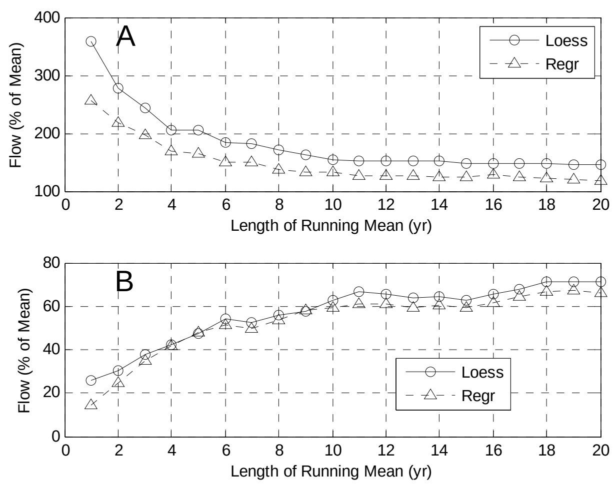

Figure 17. Extreme running means of flow reconstructed by loess curve and regression. (A) Highest running means of length 1-20 years. (B) Lowest running means of length 1-20 years. Analysis period 1541-1982.